European Journal of Medicinal Chemistry 317 (2026) 119091

Contents lists available at ScienceDirect

European Journal of Medicinal Chemistry

journal homepage: www.elsevier.com/locate/ejmech

Research paper

Pyrazinamide-derived 1,2,3-triazoles: Antimicrobial evaluation, selective antimycobacterial activity and mechanism of action insights

Priam-Amedeo Houngbedji [a,*], Andrea Bachtíková [a], Jarmila Boháčová [a], Parinaz Tabarestani [a], Ondřej Janďourek [a], Klára Konečná [a], Jan Őosterreicher [a], Pavla Paterová [b], Martin Novák [c], Pavel Bárta [a], Monika Záhorszká [d], Jana Korduláková [d], Matteo Mori [e], Fiorella Meneghetti [e], Jan Zitko [a,**]

[a] Faculty of Pharmacy in Hradec Králové, Charles University, Ak. Heyrovského 1203, Hradec Králové, 500 03, Czech Republic
[b] Department of Clinical Microbiology, University Hospital Hradec Králové, Sokolská 581, Hradec Králové, 500 03, Czech Republic
[c] Biomedical Research Centre, University Hospital Hradec Králové, Sokolská 581, Hradec Králové, 500 03, Czech Republic
[d] Department of Biochemistry, Faculty of Natural Sciences, Comenius University in Bratislava, Ilkovičova 6, Bratislava, 814 99, Slovakia
[e] Department of Pharmaceutical Sciences, University of Milan, Via Mangiagalli 25, Milan, 20133, Italy

ARTICLE INFO

Keywords:
Antimicrobial screening
Antimycobacterial
Fatty acid synthase I
Mycobacterium tuberculosis
Pyrazinamide
1,2,3-Triazole

ABSTRACT

A series of pyrazinamide-derived 1,2,3-triazoles featuring systematic chlorination of the pyrazine ring and diverse aryl substituents was synthesized and evaluated for antimycobacterial activity. Biological activity screening revealed broad-spectrum antimycobacterial activity and good selectivity toward mycobacteria over other pathogens, with 11 of the prepared compounds showing activity against *Mycobacterium tuberculosis* (Mtb) H37Ra and/or Mtb H37Rv (MIC ≤62.5 μg/mL). Structure–activity relationship analysis showed that 5-Cl substitution on the pyrazine ring was associated with improved antimycobacterial activity, with the best MIC values observed for compound **7** against Mtb H37Ra (MIC = 1.98 μg/mL) and compound **37** against Mtb H37Rv (MIC = 1.56 μg/mL). The tested compounds retained activity against drug-resistant Mtb isolates and partially against naturally resistant *Mycobacterium abscessus*, while showing low *in vitro* cytotoxicity in the HepG2 cell line and favorable selectivity indices. During advanced cytotoxicity testing, both compounds **7** and **37** displayed substantially lower hemolytic activity than bedaquiline, indicating a favorable erythrocyte safety profile within the tested concentration ranges. *In vivo* toxicity testing on *Galleria mellonella* showed low acute toxicity for both compounds. Mechanistic studies on compounds **7**, **27**, **31**, and **37** revealed reduced biosynthesis of fatty acids and derived lipids, a phenotype consistent with interference with the Fatty Acid Synthase I (FAS I) system.

1. Introduction

Tuberculosis (TB), a worldwide disease caused by *Mycobacterium tuberculosis* (Mtb), remains one of the major causes of death worldwide, with up to 10 million people developing active TB yearly, of which up to 1 million succumb to the illness [1]. The TB treatment regimens currently recommended by World Health Organization (WHO) for drug-susceptible tuberculosis remain lengthy, comprising combinations of first-line antitubercular agents (pyrazinamide, rifampicin, isoniazid, ethambutol) for 4–6 months [2]. In contrast, treatment of drug-resistant TB relies on second-line agents and is substantially longer and more complex. The rising resistance of Mtb to first-line drugs further increases the need for novel, more potent antitubercular agents [2].

Pyrazinamide (PZA) and its mechanism of action constitute the object of extensive antitubercular research [3,4]. It is understood that PZA is transformed by mycobacterial pyrazinamidase PncA into pyrazinoic acid (POA) [4], and mutations in *pncA* are the most common cause of resistance to PZA [4]. However, the antitubercular activities of PZA and POA have been linked to different mechanisms of action. Earlier studies explained the antimycobacterial activity of PZA solely as the nonspecific effect of POA acting as a protonophore, acidifying the mycobacterial cytoplasm and disrupting processes dependent on the pH gradient [4]. More recent studies indicate target-specific effects - 5-Cl PZA and other simple PZA derivatives [5] act as inhibitors of mycobacterial Fatty Acid

* Corresponding author.
** Corresponding author.
E-mail addresses: houngbepr@faf.cuni.cz (P.-A. Houngbedji), jan.zitko@faf.cuni.cz (J. Zitko).

https://doi.org/10.1016/j.ejmech.2026.119091
Received 6 April 2026; Received in revised form 21 June 2026; Accepted 22 June 2026
Available online 23 June 2026

Synthase I (FAS I) complex, and POA and 6-Cl POA are proven inhibitors of mycobacterial aspartate decarboxylase PanD [6].

Historically, many modifications of the PZA structure have been attempted, most focusing on simple modifications of the carboxamidic moiety and/or substitution of the pyrazine ring. Fig. 1 depicts examples of successful modifications, leading to compounds with low micromolar growth-inhibiting activity against Mtb. Starting from *N*-phenylpyrazine-2-carboxamides with 5-Cl, 6-Cl, 5-*tert*-butyl or other substitution of the pyrazine ring (Fig. 1, structure I, n = 0) [7–9], the other derivatives can be derived by insertion of a linker between the PZA motif and the phenyl ring. Methylene linker led to *N*-benzyl derivatives (Fig. 1, structure I, n = 1) [10]. Azomethine linker (–N═CH–) led to benzylidene hydrazide derivatives (Fig. 1, II) [11]. Compounds of general structure III already had the motif of PZA connected with a five-membered heterocycle-containing linker to a phenyl ring [12].

In this paper, we focus on the insertion of a 1,2,3-triazole linker into the structure of *N*-phenylpyrazine-carboxamide. In drug research, 1,2,3-triazole is often used as a chemically stable linker in hybrid molecules and conjugates [13]. The attractiveness of the triazole is further backed by its easy synthesis through click chemistry, a synthetic approach combining molecules as easily as a key entering its keyhole [14]. Several triazole-containing drugs are already approved in clinical practice, such as the beta-lactamase inhibitor tazobactam, the cephalosporin antibiotic cefatrizine or the antiepileptic agent rufinamide, with more in pre-clinical testing [13]. Following this trend, we proposed a series of pyrazinamide-1,2,3-triazole derivatives to explore the potential of the 1,2,3-triazole heterocycle in antitubercular research, given its utility in anti-infective drug discovery.

In our current series, the triazole linker is connected to the pyrazinamide moiety through a methylene unit, bearing structural resemblance to morphazinamide [15], which is the only PZA derivative with historical clinical usage, although marginal. The obtained compounds vary in the substitution of the pyrazine ring (R^1 = H, 3-Cl, 5-Cl, 6-Cl), and their substitution R^2 of the aryl side ring (Fig. 1, IV). The aryl is phenyl (for most of the compounds, **1**–**39**) or 1-naphthyl (**40**–**46**). Substitution R^2 was chosen to cover both electron-donating (EDG), electron-withdrawing (EWG), lipophilic and hydrophilic substituents [16,17]. Reddyrajula et al. [18] recently reported a small series of *N*-[(1*H*-1,2,3-triazol-4-yl)methyl]pyrazine-2-carboxamides structurally related to our current series. However, these compounds primarily featured an unsubstituted pyrazine core combined with electron-withdrawing substituents on the benzyl moiety. In contrast, our design introduces two deliberate structural modifications: systematic chlorination of the pyrazine ring, particularly at the 5-position, and direct attachment of the aryl substituent to the triazole ring by removing the additional methylene linker. Although this change is subtle, it reduces conformational flexibility and enables evaluation of a more rigid scaffold. Moreover, the aryl substituent set was expanded to include EWG, EDG, hydrophilic, lipophilic, and sterically demanding groups, allowing a broader SAR analysis than in the previous preliminary report.

The synthesized compounds were tested for antimycobacterial, antibacterial, and antifungal activity to assess their whole-cell inhibitory activity and selectivity. Compounds with inhibitory activity against Mtb H37Rv were selected for testing against drug-resistant Mtb clinical isolates. Based on the results, the most promising compounds were selected for *in vitro* cytotoxicity testing on HepG2 cell line and their selectivity indices (SI) were evaluated. Final compounds with the best SI for Mtb H37Ra and Mtb H37Rv were then selected for advanced cytotoxicity studies (*in vitro* hemolysis of human erythrocytes and *in vivo* cytotoxicity in *Galleria mellonella* larvae animal model). Selected compounds were assessed for their potential to influence biosynthesis of fatty acids and mycolic acids in mycobacteria, and the metabolic stability of compounds was assessed in Human Liver Microsomes (HLM).

2. Results and discussion

2.1. Chemistry

The synthesis of the target pyrazinamide-derived 1,2,3-triazoles followed the general route shown in Scheme 1. In the first step, pyrazine-2-carboxylic acids bearing different substituents on the pyrazine ring (R^1 = H, 3-Cl, 5-Cl or 6-Cl) were activated to the corresponding acid chlorides and subsequently coupled with propargylamine to afford *N*-(prop-2-yn-1-yl)pyrazine-2-carboxamide intermediates in excellent yields (85–95%) (Scheme 1A). The required aromatic azides were generated from the corresponding anilines by diazotization/azidation [14] and used directly in the following step without purification (Scheme 1B).

The final compounds were obtained by copper(I)-catalyzed azide–alkyne cycloaddition (CuAAC) between the alkyne intermediates and aromatic azides, providing the desired 1,4-disubstituted 1,2,3-triazoles (Scheme 1C). This strategy enabled efficient preparation of a structurally diverse series varying both in the substitution of the pyrazine ring and in the aryl substituent attached to the triazole moiety. The CuAAC reaction generally afforded the desired products in moderate to good yields across the series. Hydroxy-substituted derivatives proved somewhat more challenging to synthesize due to the formation of colored side products during azide generation. Naphthyl derivatives were typically isolated in lower yields (39–47%) than the corresponding phenyl analogs, which were obtained in yields of 32–85% when hydroxy-substituted derivatives were excluded.

Final compounds were isolated as solids in yields ranging from 23% to 85% (final step). Compounds were characterized by ^{1}H NMR, ^{13}C NMR, elemental analysis, melting point, IR spectroscopy (ATR-Ge) and, for selected compounds, high-performance liquid chromatography–high-resolution mass spectrometry (HPLC–HRMS) analysis. The ^{1}H NMR spectra showed the following characteristic signals: 10.53–9.19 ppm (amide N-H signal), 8.71–8.30 ppm (triazole

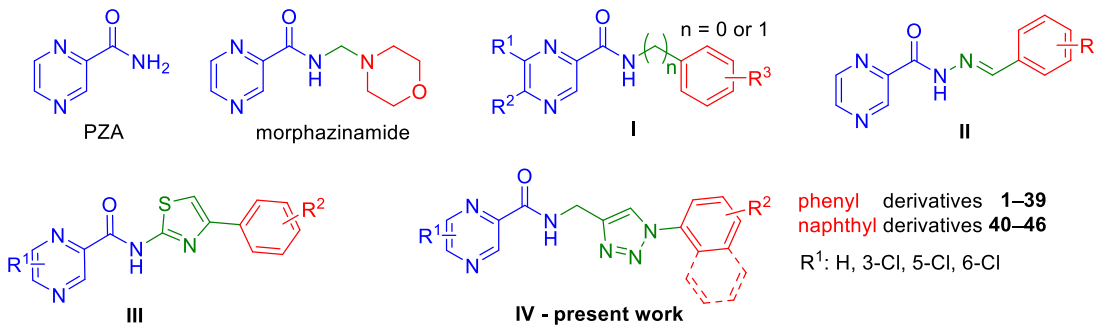

Fig. 1. An overview of structurally similar compounds previously published in the literature and our work. I: *N*-phenyl- or *N*-benzylpyrazinecarboxamides, II: pyrazinecarbohydrazides, III: *N*-((4-phenyl)aminothiazol-2-yl)pyrazine-2-carboxamides, IV: Present work, *N*-[(1-aryl-1*H*-1,2,3-triazol-4-yl)methyl]pyrazine-2-carboxamides. The pyrazinamide fragment is highlighted in blue, the linker moiety in green, and the side ring in red.

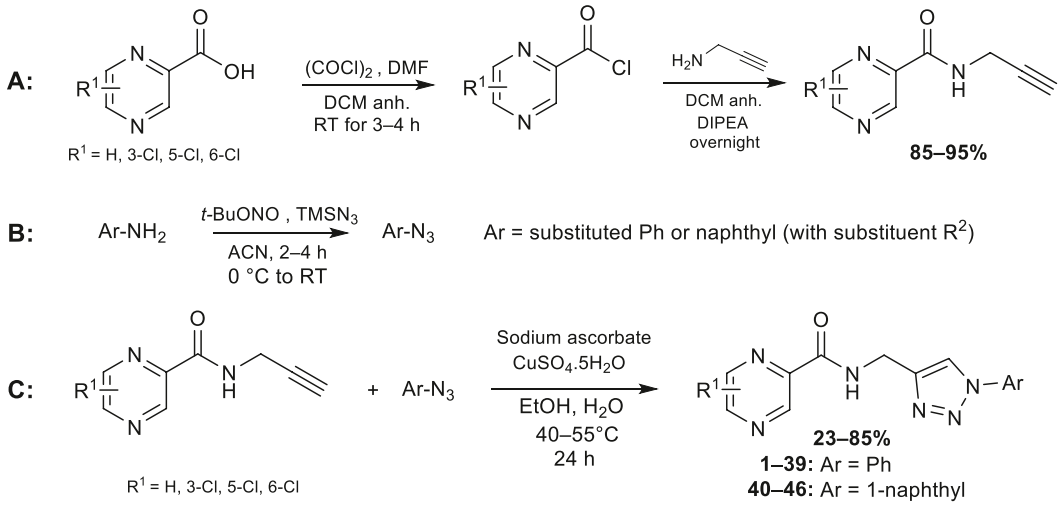

Scheme 1. Synthetic route to 1,2,3-triazole-containing pyrazinamide derivatives.

aromatic C-H signal), 4.73–4.57 ppm (methylene C-H signal). The obtained IR spectra confirmed the presence of the carboxamide moiety: 3402–3265 cm^{-1} (amide N-H stretch), 1688–1648 cm^{-1} (amide C═O stretch). All analytical data were consistent with the proposed structures (see Supplementary Material, Section 2.1).

2.2. Antimicrobial activity

2.2.1. Antimycobacterial activity – *M. smegmatis, M. aurum, M. avium, M. kansasii, M. tuberculosis H37Ra, and M. tuberculosis H37Rv*

All compounds were tested for inhibitory activity against *Mycobacterium smegmatis, Mycobacterium aurum*, *Mycobacterium avium*, *Mycobacterium kansasii*, and *Mycobacterium tuberculosis* H37Ra using a Microplate Alamar Blue Assay (MABA) [19]. The fast-growing

Table 1
Results of the primary antimycobacterial screening (compounds with activity against Mtb H37Ra or Mtb H37Rv). MIC values are in μg/mL.

Compounds				MIC[b] (μg/mL)					
No.	R^1	R^2	logP[a]	*M. smeg.*	*M. aurum*	*M. avium*	*M. kansasii*	Mtb H37Ra	Mtb H37Rv
3	5-Cl	H	1.59	≥500	125	**62.5**	**62.5**	**62.5**	**25**
5	H	2-Cl	1.25	≥500	**250**	**125**	**125**	**250**	n.a.
6	3-Cl	2-Cl	2.15	≥500	≥500	≥500	**125**	**250**	**6.25**
7	5-Cl	2-Cl	2.15	**15.63**	**31.25**	**15.63**	**7.81**	**1.98**	**50**
17	H	4-Et	1.59	≥500	≥500	≥500	**7.81**	≥500	**100**
21	H	4-OMe	0.56	≥500	≥500	250	**62.5**	≥500	**3.13**
27	5-Cl	2-OH	1.20	**7.81**	**15.63**	**31.25**	**15.63**	**3.97**	>100
30	3-Cl	4-OH	1.20	≥500	≥500	**125**	**62.5**	**125**	**6.25**
31	5-Cl	4-OH	1.20	250	≥500	≥500	250	**15.63**	**1.56**
37	5-Cl	2,6-diCl	2.71	**15.63**	**31.25**	≥500	≥500	**7.81**	**25**
38	5-Cl	2-Et	2.49	**31.25**	**31.25**	125	≥500	**31.25**	**100**
39	5-Cl	2-Me	2.08	≥500	≥500	≥500	≥500	**7.81**	n.a.
46	H	4-Br	2.51	≥500	≥500	**125**	**7.81**	**250**	0.2
INH	-	-	-	15.63	3.91	1000	6.25	0.25	n.a.
RIF	-	-	-	12.5	0.39	0.125	0.025	0.002	n.a.
CIP	-	-	-	0.125	0.016	1.56	0.25	0.25	

[a] LogP calculated by ChemDraw 22.2.0.
[b] MIC values were determined in duplicate using two-fold serial dilution. Duplicate readings for the compounds from this series were identical; Standards: INH – isoniazid; RIF – rifampicin; CIP - ciprofloxacin. n.a. – not available.

M. smegmatis and *M. aurum* are often used as surrogate models in mycobacterial research [20,21]. Non-tuberculous mycobacteria (NTM) *M. avium* and *M. kansasii* are organisms causing opportunistic infections in immunocompromised individuals, with a rapidly increasing clinical importance [22]. Mtb H37Ra is an avirulent substitute to the highly virulent Mtb H37Rv with qualitatively comparable minimum inhibitory concentrations (MIC) [23].

Compounds with activity against Mtb H37Ra or other mycobacterial strains (MIC ≤62.5 μg/mL) were tested for activity against Mtb H37Rv and *Mycobacterium abscessus*. *M. abscessus* is a rapidly growing strain with high natural resistance to antibiotics, difficult treatment, and rising incidence [24,25].

Table 1 shows the screening results of compounds which showed inhibitory activity against Mtb H37Ra or Mtb H37Rv. The compounds not presented in this table were inactive against these strains. Full results of antimycobacterial screening for all compounds are available in Supplementary material S1 (Table S6).

Firstly, we analyzed our initial series of compounds **1**–**36**, which were a combinatorial library having four different substituents on the pyrazine ring (R^1 = H, 3-Cl, 5-Cl, 6-Cl) and nine different substitutions in the phenyl part (R^2 = H, 2-Cl, 4-Cl, 4-Br, 4-Et, 4-OMe, 2-OH, 4-OH, 4-NO_2). For the discussion of results, we define compounds as highly active (MIC ≤7.81 μg/mL), moderately active (MIC 15.63–62.5 μg/mL), and inactive (MIC ≥100 μg/mL). Considering substitution R^1 on the pyrazine ring and the activity against Mtb H37Ra (surrogate for H37Rv, all compounds tested), only derivatives bearing a 5-chloro substituent exhibited activity, with 4 out of 9 compounds classified as highly active or moderately active, whereas all analogs with R^1 = H, 3-Cl, or 6-Cl were inactive. This trend remained largely consistent when considering a broader panel of mycobacterial strains, where activity (defined as MIC ≤62.5 μg/mL in at least one strain) was observed for 6/9 compounds in the 5-Cl series, compared to 3/9 for unsubstituted analogs, 1/9 for 6-Cl, and none for 3-Cl derivatives. Outside 5-Cl derivatives, activity appeared only against *M. kansasii*. However, it must be noted that from our long-term experience with this strain, it has always been the most vulnerable to growth inhibition from our panel.

Considering the R^2 substituent on the phenyl and the activity against Mtb H37Ra, only a few substituents yielded active or moderately active compounds, with 2-Cl and 2-OH being the most frequent (2/4 each), while H, 4-Cl, and 4-OH produced only a single active derivative. No activity was observed for 4-Br, 4-Et, 4-OMe, or 4-NO_2. In contrast, when considering all strains, broader activity was observed, particularly for 4-Cl and 4-Et (4/4), followed by 4-OH (3/4) and 2-Cl, 2-OH, and 4-NO_2 (2/4 each), whereas 4-OMe remained inactive. Overall, the influence of R^2 was less pronounced and more strain-dependent compared to R^1. For graphical representation of the described Structure-Activity Relationship (SAR) for compounds **1**–**36**, see the activity heatmap in Supplementary material S1, Fig. S1.

Based on the results of the first series **1**–**36,** it seemed R^1 = 5-Cl and R^2 *ortho* effect are important determinants of activity against Mtb. Therefore, we prepared and tested three more derivatives **37**–**39**, all with R^1 = 5-Cl, and R^2 was 2,6-diCl for **37**, 2-Et for **38** and 2-Me for **39**. Indeed, these compounds were active, indicating the positive effect of sterically demanding substituent R^2 in *ortho* position of the phenyl ring, possibly leading to the preference of non-coplanar conformation of phenyl relative to the triazole. To further increase the steric bulkiness of the aryl substituent on triazole, we prepared several derivatives with 4-substituted 1-naphthyl instead of phenyl (compounds **40**–**46**), but these compounds were active only against *M. kansasii* with no activity against Mtb or NTM.

Overall, the most potent compounds in the series were **7**, **27**, and **37**, which exhibited low micromolar activity against both Mtb H37Ra and H37Rv, with compound **37** showing the highest potency overall (MIC = 1.56 μg/mL against H37Rv). Notably, all three share a common structural motif consisting of a 5-chloro substituent as R^1 and an *ortho*-substituted phenyl ring at R^2 (2-Cl, 2-OH, or 2,6-diCl). In addition to their high potency, these compounds also showed the broadest spectrum of activity, being active across most of the tested mycobacterial strains, including NTM. Some *para* R^2 substituents, particularly 4-Cl and 4-Et, also contributed to a broader spectrum of activity across NTM strains, as exemplified by compounds **9**, **11**, and **12** (4-Cl) and **17**–**20** (4-Et), albeit with limited potency against Mtb.

The positive effect of 5-Cl substitution of the pyrazine ring on antimycobacterial activity is consistent with our previous series of *N*-phenyl- and *N*-benzylpyrazine-2-carboxamides [8,9]. Interestingly, in these two series, *ortho* substitution with chlorine or hydroxy group also yielded the most active compounds with MIC against Mtb H37Rv ranging 0.78–3.56 μg/mL [8,9], values aligned with the activity of our compounds **7**, **27 and 37**.

Compared with the structurally related series reported by Reddyrajula et al., [18] the present data indicate that the activity of pyrazinamide-derived 1,2,3-triazoles is not governed solely by the presence of the triazole linker and aryl substituent. Instead, within the present SAR dataset, the presence of chlorine at the 5-position of the pyrazine ring was associated with markedly improved antimycobacterial activity. This is illustrated by the substantially higher activity of 5-chloro derivatives compared with unsubstituted, 3-chloro, and 6-chloro analogs. In addition, the expanded aryl-substituent set enabled identification of the 2-hydroxy derivative (**27**) as one of the most balanced compounds in terms of activity and selectivity, demonstrating that favorable activity is not restricted to strongly electron-withdrawing aryl substituents. Thus, despite the structural relationship to the previously reported compounds, the present series provides additional SAR information on both the pyrazine and aryl portions of the scaffold.

2.2.2. Antimycobacterial activity – drug-resistant Mtb isolates and naturally resistant M. abscessus

The compounds active against Mtb H37Rv were advanced for screening of inhibitory activity against drug-resistant Mtb isolates and naturally resistant *M. abscessus* (Table 2). Compounds **7** and **37** were also tested against clinical isolates Mtb Praha 131, 9449/2007 and 8666/2010 (Table 3). The resistance profiles of clinical isolates are available in Supplementary material S1, Table S1. Importantly, all tested compounds retained at least partially their activity against the tested clinical isolates with compound **37** showing the most potent inhibitory activity.

2.2.3. Antibacterial and antifungal activity

All final compounds were screened for *in vitro* antibacterial and antifungal activities. The full results are available in Supplementary material S1, Tables S7 and S8. The testing of compounds **3**, **13**, **19**, **20**, **28**, **40**, **41**, **42**, **43** and **45** was not possible due to precipitation in testing media.

The antibacterial activity was tested against *Staphylococcus aureus* (SA), methicillin-resistant *Staphylococcus aureus* (MRSA), *Staphylococcus epidermidis* (SE), *Enterococcus faecalis* (EF), *Escherichia coli* (EC), *Klebsiella pneumoniae* (KP), *Acinetobacter baumannii* (ACI) and *Pseudomonas aeruginosa* (PA). Several compounds showed mild inhibitory activity (MIC 62.5–125 μM) against SA and SE as summarized in Table 4. No other antibacterial activity was observed against the selected bacterial strains within the tested range; Gram-negative bacteria were not affected. For full results, see Supplementary material S1, Table S7.

It appears that chlorination on the pyrazine ring in phenyl series improves activity against **SA** and **SE** more than the substitution on the aromatic side ring. 3-Cl substitution gives active compounds more frequently than other substitutions, as opposed to 5-Cl substitution for antimycobacterial activity. Surprisingly, the best results were obtained with the 4-NO_2 substituted naphthalene ring containing compound **44**.

None of the tested molecules showed antifungal activity when tested against *Candida albicans*, *Candida krusei*, *Candida parapsilosis*, *Candida tropicalis*, *Aspergillus fumigatus*, *Aspergillus flavus*, *Lichtheimia corymbifera*,

Table 2
Antimycobacterial activity against drug-resistant Mtb isolates and naturally resistant *M. abscessus*. MIC values are in μg/mL.

Cmpd	MIC[b] (μg/mL)						
	Mtb MATI	Mtb SORO	Mtb TIAS	Mtb YAGY	Mtb TURZ	Mtb H37Rv	*M. abscessus*
3	12.5	25	25	25	50	25	>100
7	6.25	>100	12.5	3.13	>100	6.25	25
17	12.5	25	25	12.5	12.5	50	>100
21	50	50	50	25	50	100	>100
27	3.13	6.25	6.25	6.25	12.5	3.13	25
31	6.25	12.5	6.25	6.25	6.25	6.25	100
37	1.56	3.13	6.25	6.25	3.13	1.56	25
38	25	25	25	50	25	25	50
39	6.25	12.5	25	>100	50	100	>100
INH	>6.25 R	6.25 R	6.25 R	>6.25 R	>6.25 R	0.20	>6.25
RIF	>0.78 R	0.10	0.05	>0.78 R	>0.78 R	0.10	>0.78
EMB	0.20	0.39	0.10	0.39	0.39	0.05	>0.78
WHO classification[a]	MDR-TB	INH-monoresistant TB		MDR-TB	MDR-TB	drug-sensitive	naturally resistant

[a] WHO resistance classification according to post-2021 WHO definitions: MDR-TB is resistant to at least isoniazid and rifampicin.
[b] MIC values were determined in duplicate using two-fold serial dilution. Duplicate readings for the compounds from this series were identical; R – Resistant. INH – isoniazid; RIF – rifampicin; EMB - ethambutol.

Table 3
Antimycobacterial activity of compounds **7** and **37** against drug-resistant Mtb isolates Praha 131, 9449/2007 and 8666/2010. Results are evaluated after 14 and 21 days of incubation at 37°C and expressed as MIC in μM (μg/mL).

No.	MIC[b] μM (μg/mL)					
	Mtb Praha 131		Mtb 9449/2007		Mtb 8666/2010	
	14d	21d	14d	21d	14d	21d
7	64 (22.35)	250 (87.29)	64 (22.35)	64 (22.35)	16 (5.59)	32 (11.17)
37	32 (12.28)	32 (12.28)	16 (6.14)	16 (6.14)	32 (12.28)	32 (12.28)
INH	16 R		64 R		32 R	
RIF	>8 R		>8 R		>8 R	
OFX	16 R		2		8 R	
WHO classification[a]	pre-XDR-TB		MDR-TB		pre-XDR-TB	

[a] WHO resistance classification according to post-2021 WHO definitions: **RR-TB** is rifampicin-resistant tuberculosis; **MDR-TB** is resistant to at least isoniazid and rifampicin; **pre-XDR-TB** is MDR/RR-TB with additional resistance to any fluoroquinolone.
[b] MIC values were determined in duplicate using two-fold serial dilution. Duplicate readings for the compounds from this series were identical; R – resistant. INH – isoniazid, RIF – rifampicin, OFX - ofloxacin.

Table 4
Antibacterial activity of compounds active against *Staphylococcus aureus* (SA) and *Staphylococcus epidermidis* (SE). The results are expressed as MIC (μM).

Compound			MIC[a] (μM)			
			SA		SE	
No.	R^1	R^2	24h	48h	24h	48h
2	3-Cl	H	**125**	**125**	**62.5**	**62.5**
6	3-Cl	2-Cl	>500	>500	**500**	**500**
14	3-Cl	4-Br	**125**	>125	**125**	**125**
16	6-Cl	4-Br	**125**	>125	**125**	>125
18	3-Cl	4-Et	>125	>125	**125**	>125
26	3-Cl	2-OH	**500**	>500	**250**	**500**
27	5-Cl	2-OH	**250**	**500**	**250**	**250**
36	6-Cl	4-NO_2	**125**	**125**	>125	>125
37	5-Cl	2,6-diCl	**125**	**125**	>125	>125
38	5-Cl	2-Et	**125**	**125**	>125	>125
44	H	4-NO_2	**62.5**	**125**	**31.25**	**62.5**
46	H	4-Br	**125**	**125**	>125	>125
CIP	-	-	0.39	-	>3.09	-
GEN	-	-	2.09[b]	-	>16.75[b]	-

[a] MIC values were determined in duplicate using two-fold serial dilution. Duplicate readings for the compounds from this series were identical.
[b] For conversion purposes, an average molecular weight of ~478 g/mol was used for GEN, which is a mixture of related aminoglycosides; CIP – ciprofloxacin, GEN – gentamicin.

Trichophyton interdigitale within the tested range, see Table S8 in Supplementary material.

2.3. Evaluation of toxicity

2.3.1. In vitro cytotoxicity in HepG2 and HK-2 cells

Pivotal compounds with promising activity against Mtb H37Ra and Mtb H37Rv were selected for cytotoxicity testing on human hepatocellular carcinoma cell line (HepG2). The HepG2 cell line is commonly used in the early evaluation of antitubercular compounds, as any newly developed anti-TB agent will likely be incorporated into combination treatment regimens that already include drugs with considerable hepatotoxic potential [26]. Testing results are displayed in Table 5 as IC_{50} (μM) along with the calculated selectivity indices SI.

The active compounds showed low cytotoxicity with IC_{50} values close to or higher than 100 μM. Compounds **7**, **27**, **31**, and **37** met the commonly applied criterion SI > 10. Relative to HepG2, the best SI values were seen with compound **7** for Mtb H37Ra (H37Ra $SI_7 = \mathbf{18.71}$) and compound **37** for Mtb H37Rv (H37Rv $SI_{37} = \mathbf{22.80}$).

Compounds **7**, **27**, **31**, and **37** (SI > 10 based on HepG2 cytotoxicity) were further evaluated for cytotoxicity in the non-cancerous human HK-2, an immortalized human proximal tubular epithelial cell line derived from normal kidney tissue (Table 5). All tested compounds exhibited higher cytotoxicity toward HK-2 cells than toward HepG2 cells. The relatively higher HK-2 cytotoxicity observed for compounds **7** and **37** compared with compounds **27** and **31** may be, at least in part, attributed to their higher degree of chlorination and consequently increased lipophilicity, which may promote nonspecific interactions with cellular membranes or intracellular targets. Among the compounds tested, compound **37** displayed the highest cytotoxicity toward HK-2 cells.

Table 5
The antimycobacterial activity of selected compounds as MIC (μM) next to their cytotoxicity on HepG2 and HK-2cell lines as IC_{50} (μM) and the calculated selectivity index SI.

Compound			MIC (μM)[a]		IC_{50} (μM)	SI relative to HepG2		IC_{50} (μM)	SI relative to HK-2	
No.	R^1	R^2	Mtb H37Ra	Mtb H37Rv	HepG2	IC_{50}/MIC_{H37Ra}	IC_{50}/MIC_{H37Rv}	HK-2	IC_{50}/MIC_{H37Ra}	IC_{50}/MIC_{H37Rv}
3	5-Cl	H	198.58	79.43	83.0	0.42	1.04			
7	5-Cl	2-Cl	5.67	17.90	106.1	**18.71**	5.92	59.1	10.42	3.30
27	5-Cl	2-OH	12.00	9.46	170.9	**14.24**	**18.07**	154.5	12.88	16.33
30	3-Cl	4-OH	377.95	≥302.36	≥1000	≥2.65	≥3.30			
31	5-Cl	4-OH	47.24	18.90	205.0	4.34	**10.85**	88.6	**1.88**	**4.69**
37	5-Cl	2,6-diCl	20.36	4.07	92.8	4.56	**22.80**	25.8	**1.27**	**6.34**
38	5-Cl	2-Et	91.16	72.93	134.4	1.47	1.84			
39	5-Cl	2-Me	23.76	339.77	82.4	3.47	0.24			

[a] MIC values in μM were calculated from values in μg/mL reported in Table 1.

Compounds **7**, **27**, **31**, and **37** (SI > 10 based on HepG2 cytotoxicity against at least one of the tested mycobacterial strains) were directly advanced to mechanism-of-action studies (Section 2.4). Compounds exhibiting borderline selectivity (**7**) or unsatisfactory selectivity in HK-2 cells (**37**) were additionally subjected to advanced toxicity testing to better assess their toxicity potential (Sections 2.3.2 and 2.3.3).

2.3.2. *Ex vivo hemolysis assay using human erythrocytes*

Evaluation of hemolytic activity toward human erythrocytes was performed as an initial safety assessment to identify potential membrane-disruptive effects of compounds **7** and **37** (Fig. 2). Erythrocyte hemolysis is a commonly used surrogate marker of blood-cell toxicity and provides an early indication of systemic tolerability [27]. At the highest achievable concentration in the aqueous phase, compound **37** exhibited statistically higher hemolytic activity than compound **7**. For both compounds, statistically significant hemolysis within the tested concentration range was observed only at 500 μM. The reference drug bedaquiline, a clinically approved antitubercular drug used for the treatment of MDR-TB, induced statistically significant hemolysis already at 125 μM. Overall, both compounds **7** and **37** displayed substantially lower hemolytic activity than bedaquiline, indicating a more favorable biocompatibility with human blood within the tested concentration range.

2.3.3. *In vivo toxicity– Galleria mellonella animal model*

The acute *in vivo* toxicity of pivotal compounds **7** and **37** was evaluated using the invertebrate larvae animal model of *Galleria mellonella* [28]. The compounds were administered in a single dose via intra-hemocoel administration. Larvae were divided into groups according to the final amount of administered compound per kg of body weight (1500 mg/kg, 500 mg/kg, 50 mg/kg). After administration, the mortality of larvae was monitored for five days. See section 2.6 in Supplementary material S1 for full methodology and statistical results (Tables S9 and S10). As illustrated in Fig. 3, compound **7** showed a higher toxic potential compared to compound **37** at doses of 500 and 1500 mg/kg body weight. At the highest tested concentration (1500 mg/kg body weight), compound **7** induced the highest animal mortality, reaching 40% within 24 h post-administration. For compound **37**, the highest mortality was observed 48 h after administration and reached 20%. At 50 mg/kg, no death was observed for either of the compounds. In conclusion, LD_{50} was not reached for either compound at maximal tested concentration and both compounds can be classified as Globally Harmonized System (GHS) category 4, corresponding to low toxicity.

2.4. *Mechanism of action (MoA)*

2.4.1. *The effect of compounds **7**, **27**, **31** and **37** on mycolic acids and lipids synthesis of M. tuberculosis H37Ra*

5-Chloropyrazine-2-carboxamide inhibits the mycobacterial Fatty Acid Synthase I (FAS I) system by binding to the NADPH binding site, with an affinity superior to that of unsubstituted PZA [9,29,30]. Since our series combine the pyrazine-2-carboxamide moiety with a 1,2,3-triazole-phenyl moiety, and the majority of compounds with 5-Cl

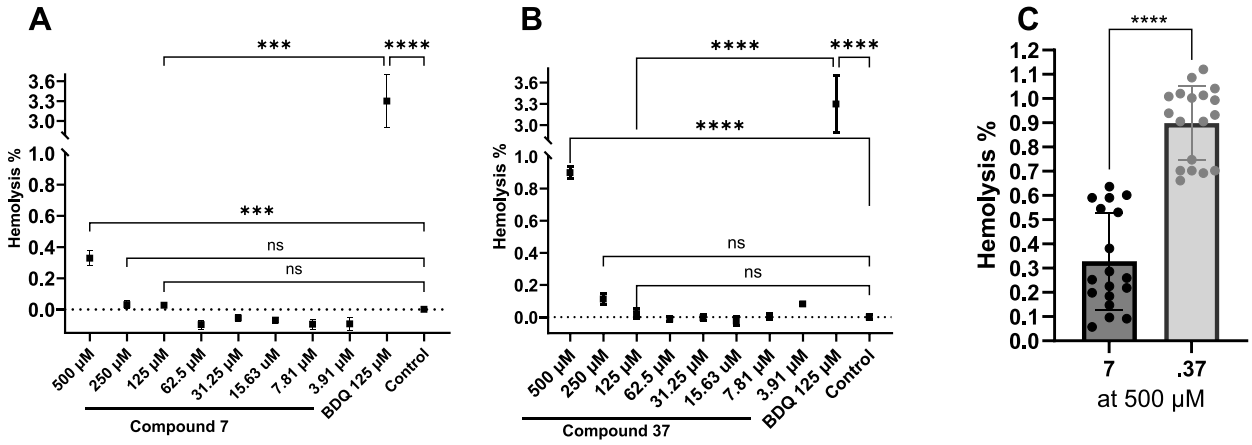

Fig. 2. Evaluation of the hemolytic activity of compounds **7** (**A**) and **37** (**B**) in comparison with bedaquiline. Hemoglobin release into the supernatant was measured at 405 nm. Data were corrected for the negative control (unexposed erythrocytes) and are expressed as the mean ± SEM (n = 18). Statistical significance was determined using a nonparametric one-way ANOVA (Kruskal–Wallis test). (C) Detailed comparison at 500 μM evaluated by *t*-test: $p < 0.05$ (*); $p < 0.01$ (**); $p < 0.001$ (***); $p < 0.0001$ (****).

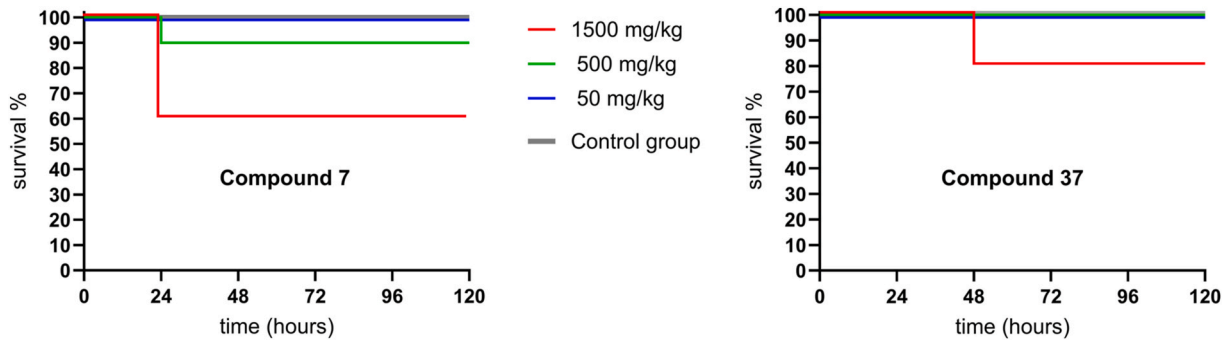

Fig. 3. Survival curves of animal model, *Galleria mellonella,* after intra-hemocoel administration of compounds **7** and **37**. After single-dose administration, larvae were incubated at 37°C for five days and inspected after 24, 48, 72, 96 and 120 h of incubation.

substitution on the pyrazine ring show good antimycobacterial activity, we hypothesized that the mechanism of action could involve disruption of mycolic acids or lipids synthesis through interaction with the FAS I system. Moreover, structurally related 1,2,3-triazole-containing derivatives of PZA were suggested, based on molecular docking studies, to inhibit the mycobacterial enoyl-ACP-reductase (InhA), a key enzyme of the FAS II system [18]. Therefore, we employed our well-established methodology to evaluate the effects of the studied compounds on the biosynthesis and composition of lipids, fatty acids, and mycolic acids in the model organism of Mtb H37Ra. Interference with either FAS I or FAS II system would be expected to result in quantitative and/or qualitative alterations in the lipid and mycolic acid profiles.

Mtb H37Ra cells were cultivated in the presence of [^{14}C]-acetate and treated with varying multiples (×1, ×10, ×100) of the MIC of compounds **7**, **27**, **31** and **37**. TLC analysis of the radiolabeled lipids (Fig. 4) revealed that, even at 1 × MIC, all tested compounds caused a decrease in the synthesis of standard fatty acids, which in turn decreased the production of all lipids made of these acids, including triacylglycerols, phosphatidylethanolamine, cardiolipin, phosphatidylinositol and its derivatives. The synthesis of mycolic acids, trehalose dimycolates (TDM), and trehalose monomycolates (TMM) remained unaffected, except in the case of compound **31**, where inhibition was observed at 10 × MIC. The observed alterations in standard fatty acid synthesis can be linked to the inhibition of the FAS I system.

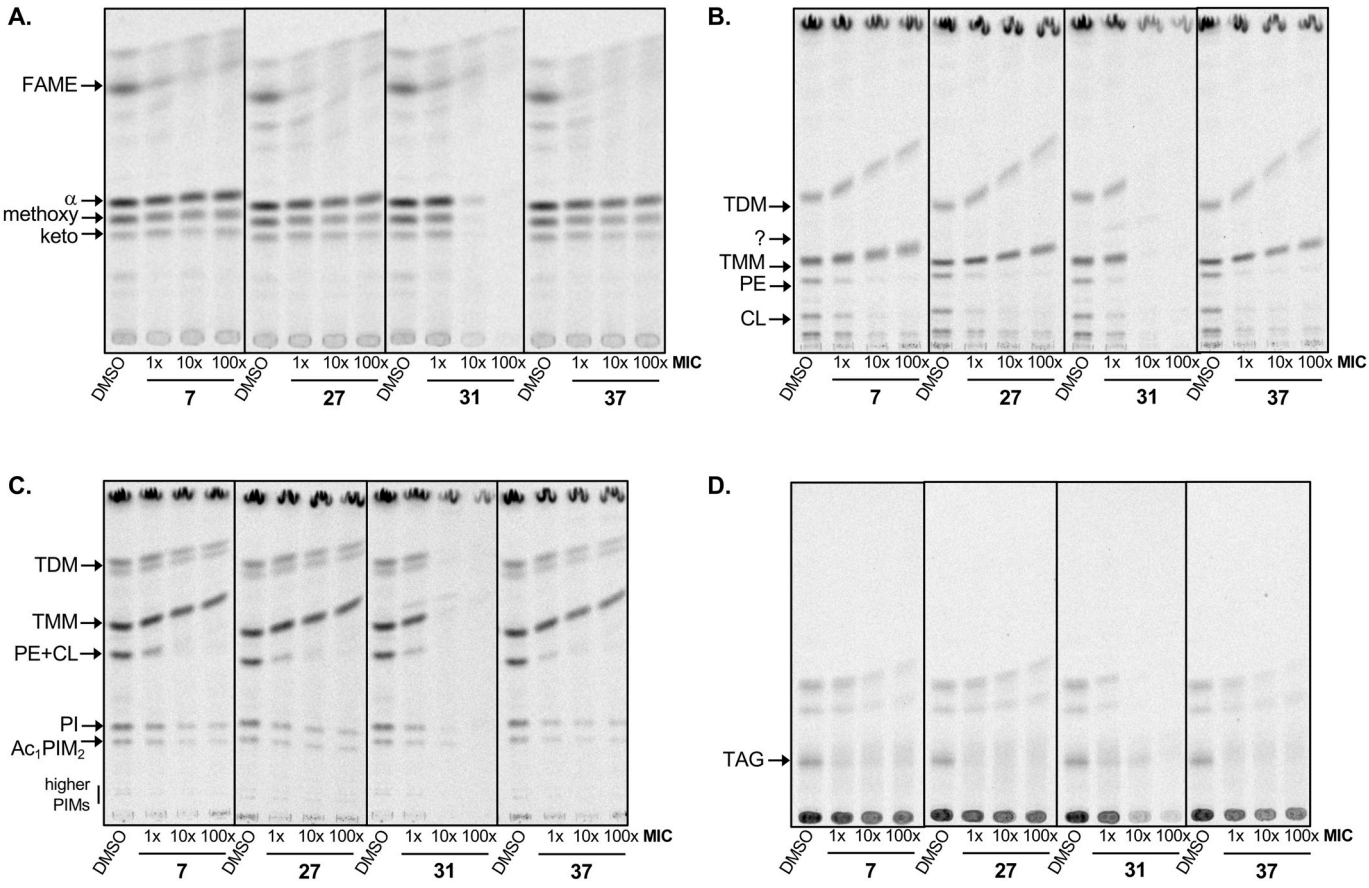

Fig. 4. The effect of compounds **7**, **27**, **31** and **37** on mycolic acids and lipids synthesis of Mtb H37Ra. (A) TLC analyses of fatty and mycolic acid methyl esters separated in *n*-hexane/EtOAc (95:5, 3x). TLC analyses of lipids separated in (B) chloroform/methanol/water (20:4:0.5); (C) chloroform/methanol/ammonium hydroxide/water (65:25:0.5:4) and (D) petroleum ether/EtOAc (98:2, 3x). FAME, fatty acid methyl esters; MAME, mycolic acid methyl esters; α, α′ and epoxy refer to forms of MAME; TDM, trehalose dimycolates; TMM, trehalose monomycolates; PE, phosphatidylethanolamine; CL, cardiolipin; Ac_1PIM_2, monoacylated phosphatidylinositol dimannosides; PI, phosphatidylinositol; TAG, triacylglycerols.

The impact of compound **31** on the synthesis of mycolic acids, TDM and TMM could be explained by different theories. One possibility is that Mtb H37Ra cells could have lost their overall metabolic activity in response to the high concentration of the inhibitor. Another explanation could be that compound **31** may also inhibit enzymes of the FAS II system, possibly targeting the enoyl-ACP reductase InhA. It is also possible that compound **31** interacts with enzymes outside the FAS I/II systems, which could explain the appearance of an unidentified lipid migrating above TDM in the TLC analysis.

2.4.2. Determination of the MIC of compounds *7, 27, 31* and *37* against *Mtb H37Ra overproducing enzymes of the FAS II system*

To further investigate whether the tested compounds affect the FAS II system, we determined their MIC against Mtb H37Ra strains overproducing key FAS II enzymes, including enoyl-ACP reductase InhA [31,32] and β-hydroxyacyl-ACP dehydratase complex (HadABC) [33]. The obtained MIC values are displayed in Table 6.

The obtained MIC values indicate that overproduction of important components of FAS II system, namely InhA or the HadABC complex, does not increase resistance to the tested compounds compared with control strains harboring the empty vectors pVV2 or pMV261. These results demonstrate that the mechanism of action of the studied compounds is not related to the FAS II system. Hence, the activity profile of compounds 7, 27, and 37 is consistent with interference with FAS I-dependent fatty acid biosynthesis, although direct biochemical inhibition of purified FAS I remains to be confirmed. In contrast, the alternative mechanism underlying the activity of compound **31** remains unknown.

2.4.3. Final considerations of the mechanism of action

Our data indicate that compounds **7**, **27** and **37** inhibit fatty acid biosynthesis while not significantly affecting downstream production of mycolic acids. This is consistent with selective inhibition of the FAS I system while preserving FAS II activity. This interpretation is further supported by target overexpression experiments, in which strains overproducing key FAS II enzymes, including the enoyl-ACP reductase InhA and the dehydratase complex HadABC, did not exhibit increased resistance to the tested compounds. These findings argue against a mechanism involving FAS II and instead support the FAS I complex as the plausible target.

Mycobacterial FAS I is a large multidomain megasynthase comprising six core catalytic domains acyltransferase (AT), enoyl reductase (ER), dehydratase (DH), malonyl/palmitoyl transferase (MPT), ketoreductase (KR), and β-ketoacyl synthase (KS). The acyl carrier protein (ACP) domain dynamically shuttles reaction intermediates between the individual catalytic sites. The enzyme assembles into a massive oligomeric complex with a characteristic barrel-like architecture [34]. Several cryo-EM structures of mycobacterial FAS I have been deposited in recent years [35,36], including near-atomic resolution models such as pdb id: 9PQX [34]. In principle, these structures allow atomistic simulations, such as molecular docking or molecular dynamics.

Comprehensive structure-based simulations of our compounds with the FAS I complex are beyond the scope of this study due to its size and complexity of the system, considering multiple catalytic domains and potential allosteric sites. Based on previous biochemical reports that derivatives of 5-Cl-PZA compete with NADPH binding at mycobacterial FAS I [37], the reductive domains, particularly ER and KR, might be worth prioritization as targets. Both domains utilize nicotinamide cofactors (NADPH/$NADP^+$) and contain well-defined cofactor-binding pockets suitable for small-molecule interaction. Nevertheless, although the present results are consistent with FAS I involvement, direct biochemical inhibition of purified mycobacterial FAS I remains to be experimentally validated.

2.5. Determination of microsomal stability of compounds *7* and *37*

Compounds **7** and **37** were incubated with human liver microsomes (HLM) to obtain their microsomal stability (Table 7). The concentrations of the parent compounds were determined at specific incubation time points by HPLC-HRMS. The calculated microsomal half-life ($t_{1/2}$) and intrinsic clearance (CL_{int}) of tested compounds indicate high values of microsomal stability in comparison with diazepam (drug endowed with high microsomal stability) and verapamil (drug known for low microsomal stability). Both tested compounds can be classified as compounds with low clearance with respect to phase I metabolic deactivation. The high microsomal stability of compounds **7** and **37** is encouraging for further development, as it indicates that the triazole-containing pyrazinamide scaffold is not rapidly degraded under phase I metabolic conditions. Nevertheless, future pharmacokinetic studies will be required to determine whether this *in vitro* stability translates into favorable systemic exposure, half-life, and overall *in vivo* pharmacokinetic behavior.

2.6. In silico prediction of physicochemical properties and drug-likeness

Basic physicochemical properties of the synthesized compounds were estimated using SwissADME (see Table S15, Supplementary material S1, and Supplementary material S2 for a csv format) to assess their physicochemical profile relevant to further optimization. The series occupies a drug-like chemical space, with moderate molecular weights (~280–390 g/mol), lipophilicity (consensus logP ~1.0–2.5), and polar surface area (TPSA ~85–106 $Å^2$). Predicted aqueous solubility (ESOL) values ranged from approximately logS = −2.0 to −4.0, corresponding to soluble to moderately soluble compounds. All compounds comply with common drug-likeness rules (Lipinski, Ghose, Veber, Egan, and Muegge).

These data are useful for interpreting the SAR of the series. The most active compounds, including **7**, **27**, and **37**, do not appear to achieve activity at the cost of excessive molecular size, polarity, or lipophilicity. At the same time, the higher cytotoxicity observed in HK-2 cells for the more chlorinated/lipophilic compounds, especially compound **37**, suggests that further optimization should avoid a simple increase in lipophilicity and should instead aim to preserve antimycobacterial potency while maintaining balanced polarity and solubility. Thus, the in silico physicochemical assessment provides a supportive framework for prioritizing future analogs, although full ADME and pharmacokinetic properties will require experimental validation.

Table 6
The results of MIC determination of compounds **7**, **27**, **31**, **37** against Mtb H37Ra strains overproducing enzymes of the FAS II system, InhA or HadABC complex.

	MIC (μg/mL)			
	7	27	31	37
pVV2[a]	2	2	4	1
pVV16-*hadABC*	2	2	2	1
pMV261[a]	4	4	2–4	1
pMV261-*inhA*	2	2	2–4	1

[a] Empty vectors.

Table 7
Determination of microsomal stability. The stability is represented by HLM half-life ($t_{1/2}$) and intrinsic clearance (CL_{int}).

Compound	HLM $t_{1/2}$ (min)	CL_{int} (μL/min/mg protein)
7	301.30	4.60
37	577.50	2.40
Diazepam	301.30	4.60
Verapamil	15.40	90.09

2.7. Crystallography studies on compound **37**

The structure of compound **37** was elucidated by single-crystal X-ray diffraction to unambiguously confirm its molecular identity and gain detailed insight into the three-dimensional features of this class. Colorless prisms were obtained by slow evaporation of a methanol/diisopropyl ether solution of **37** at room temperature. The compound crystallized in the monoclinic $P2_1/c$ space group. Its molecular structure is illustrated in Fig. 5 as a thermal-ellipsoid diagram.

Structurally, the molecule can be described as consisting of three fragments, each defining a distinct mean plane. The pyrazine core, coplanar with its 2-amide moiety, is inclined at 79.0° relative to the triazole, which in turn forms an angle of 68.3° with the dichlorophenyl substituent. More detailed description of the structure, including crystal packing and intermolecular interactions, is in Supplementary material S1, section 2.7.

3. Conclusions

A series of *N*-[(1-aryl-1*H*-1,2,3-triazol-4-yl)methyl]pyrazine-2-carboxamides was synthesized using click chemistry. Of the 46 compounds prepared, 11 showed activity against Mtb H37Ra and/or H37Rv (MIC ≤62.5 μg/mL). The results demonstrated that 5-chloro substitution on the pyrazine ring markedly enhances antimycobacterial activity compared to unsubstituted, 3-chloro, or 6-chloro analogs, particularly in combination with *ortho*-substitution on the phenyl ring (R^2 = 2-Cl, 2,6-diCl, 2-OH, 2-Me, 2-Et). The most potent compounds were **7** (R^1 = 5-Cl, R^2 = 2-Cl; MIC Mtb H37Ra = 1.98 μg/mL) and **37** (R^1 = 5-Cl, R2 = 2,6-diCl; MIC Mtb H37Rv = 1.56 μg/mL). In contrast, only weak activity was observed against *Staphylococcus aureus* and *Staphylococcus epidermidis*, while Gram-negative bacteria and fungal strains were not affected within the tested concentration range, indicating a high degree of selectivity for mycobacteria.

The active compounds retained activity against drug-resistant Mtb strains and showed low cytotoxicity in HepG2 cells, with selectivity indices SI > 10 observed for compounds **7**, **27**, **31** and **37**. Hence, these compounds were selected for further cytotoxicity testing in HK-2 human kidney cells. HK-2 cytotoxicity testing revealed a moderate increase in cytotoxicity for all tested compounds, with compounds bearing additional chlorine substituents on the phenyl ring (**7** and **37**) displaying lower IC_{50} values than the hydroxy-substituted analogs **27** and **31**. Because compounds **7** and **37** remained the most potent antimycobacterial agents despite this trend, they were selected for advanced toxicity studies. In these studies, both compounds **7** and **37** displayed substantially lower hemolytic activity than bedaquiline, indicating a favorable erythrocyte safety profile. The *Galleria mellonella in vivo* model further confirmed low acute toxicity following intrahemocoel administration, consistent with GHS category 4. Both compounds also exhibited high microsomal stability in human liver microsomes ($t_{1/2}$ = 301.30 and 577.50 min, respectively). Mechanistic studies further showed that compounds **7**, **27**, **31**, and **37** affect fatty acid and lipid biosynthesis. For compounds **7**, **27**, and **37**, the observed profile is consistent with interference with FAS I-dependent fatty acid biosynthesis, whereas additional studies will be required to confirm FAS I as the direct molecular target.

Overall, this study identifies pyrazinamide-derived 1,2,3-triazoles as readily accessible compounds with selective antimycobacterial activity and provides clear SAR evidence for the beneficial role of 5-chloro substitution on the pyrazine ring combined with ortho-substitution on the phenyl ring. Among the synthesized compounds, **7** and **37** showed the highest antimycobacterial potency, while compound **27** emerged as a particularly balanced analog with favorable activity and selectivity. The biological and mechanistic data support this scaffold as a promising starting point for further optimization, although confirmation of the direct molecular target and comprehensive *in vivo* pharmacological evaluation will be required.

4. Experimental

4.1. Chemistry

4.1.1. General

All reagents and solvents (unless stated otherwise) were purchased from Merck (Darmstadt, Germany) or Fluorochem (Hadfield, UK) and used without purification. Reaction progress and purity of products were monitored using Silica 60 F_{254} TLC plates (Merck). The NMR spectra were recorded on a Varian VNMR S500 (Varian, Palo Alto, CA, USA) at 500 MHz for ^{1}H and 126 MHz for ^{13}C or a Jeol JNM-ECZ600R (JEOL, Tokyo, Japan) at 600 MHz for ^{1}H and 151 MHz for ^{13}C. The spectra were recorded in DMSO-d_6 at ambient temperature. The chemical shifts reported as δ values in ppm are indirectly referenced to tetramethylsilane (TMS) via the solvent signal (2.49 for ^{1}H and 39.7 for ^{13}C). IR spectra were recorded on a NICOLET 6700 FT-IR spectrophotometer (Nicolet, Madison, WI, USA) using the ATR-Ge method. Elemental analysis was done on a Vario MICRO cube Element Analyzer (Elementar Analysensysteme, Hanau, Germany) with values given as a percentage. Compounds **3**, **7**, **27**, **31**, **37**, **38** and **39** were analyzed by HPLC-HRMS using Dionex Ultimate 3000 UHPLC RS controlled by Chromeleon (version 7.2.9. Build 11323) software (Thermo Fisher Scientific, Bremen, Germany) connected to Q Exactive Plus Orbitrap mass spectrometer with Thermo Xcalibur (version 3.1.66.10.) software (Thermo Fisher Scientific). Yields are stated in percentage and refer to the amount of pure product after all purification steps. Melting points were determined in open capillary on a Stuart SMP30 melting point apparatus (Bibby

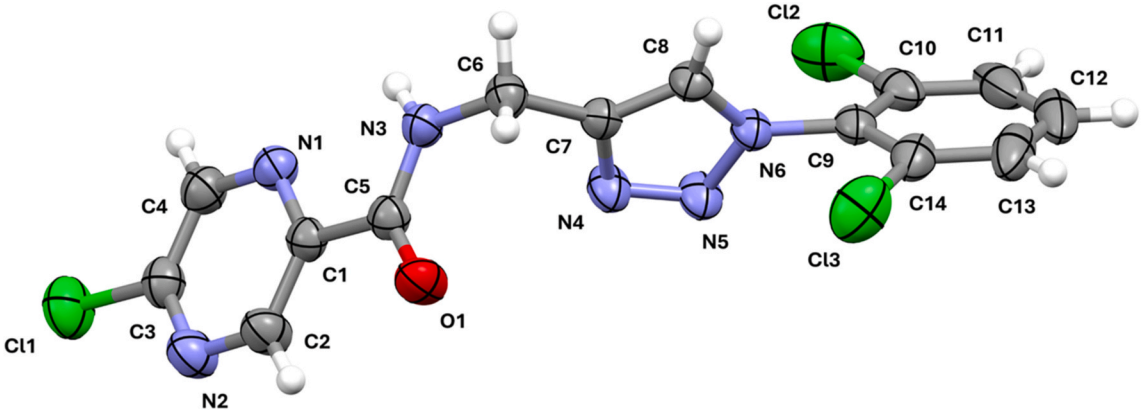

Fig. 5. Thermal-ellipsoid diagram of compound **37**, with the arbitrary atom-numbering scheme used in the discussion. Displacement ellipsoids are drawn at the 40% probability level.

Scientific Limited, Staffordshire, UK) and are uncorrected. Log*P* values were calculated using ChemDraw v22.2.0 (Revvity Signals Software, Waltham, MA, USA).

4.1.2. Procedures of chemical synthesis

4.1.2.1. Synthesis of N-(prop-2-yn-1-yl)pyrazine-2-carboxamides (procedure A)

4.1.2.1.1. Activation of pyrazinoic acid (procedure A1). Pyrazinoic acid (3 mmol, 1 eq) was dissolved in 15 mL DCM in a 100 mL round-bottomed flask, and the solution was stirred for 5 min in an ice bath (0°C). After the solution was cooled, oxalyl chloride (3.6 mmol, 1.2 eq) was added dropwise, followed by a few drops of dimethylformamide (2–3 drops). The mixture was left to stir at room temperature for 3–4 h. The reaction progress was monitored by TLC (*n*-hexane/EtOAc 1:1).

4.1.2.1.2. Acylation (procedure A2). After the activation of the respective pyrazinoic acid was complete, DIPEA (4.5 mmol, 1.5 eq) was added directly to the reaction mixture, followed by propargylamine (4.5 mmol, 1.5 eq). The reaction mixture was stirred overnight at room temperature. After completion, as confirmed by TLC (*n*-hexane/EtOAc 1:1), DCM was evaporated under reduced pressure. The obtained residue was suspended in water and extracted with EtOAc (3 x 150 mL). The combined organic fractions were washed with brine (1 x 100 mL) and dried over anhydrous Na_2SO_4. The crude product after solvent evaporation was purified by flash chromatography (gradient elution, from 100% *n*-hexane to 100% EtOAc over 45 min) to yield pure *N*-(prop-2-yn-1-yl)pyrazine-2-carboxamide as a white powder (yield 95–98%).

4.1.2.2. Synthesis of aromatic azides (procedure B).

The respective aniline (1 mmol, 1 eq) was dissolved in 15 mL of ACN in a 100 mL round-bottomed flask. The solution was cooled in an ice bath (0°C) and *tert*-butylnitrite (*t*-BuONO, 3 eq) was added dropwise followed by trimethylsilyl azide ($TMSN_3$, 2.4 eq). The reaction mixture was stirred at room temperature for 3–4h. The reaction progress was monitored by TLC (*n*-hexane/EtOAc 1:1). After completion, the reaction solvent and reagents were evaporated under reduced pressure, and the obtained crude azide was used for the following click reaction without purification.

4.1.2.3. Synthesis of 1,2,3-triazole containing pyrazinamide derivatives (procedure C)

4.1.2.3.1. Synthesis of Cu^I catalyst (procedure C1). A 50 mL round-bottomed flask was charged with sodium ascorbate (0.5 eq relative to azide) and $CuSO_4.5H_2O$ (0.125 eq relative to azide) in 5 mL of H_2O and the solution was stirred for 5–10 min (until permanent orange color).

4.1.2.3.2. Synthesis of 1,2,3-triazole by click chemistry (procedure C2). The crude azide obtained from the azide synthesis was dissolved in EtOH (20 mL per mmol), the corresponding *N*-(prop-2-yn-1-yl)pyrazine-2-carboxamide (0.83 eq of azide) was added, and the mixture was stirred for 5 min at room temperature. The previously prepared Cu^I catalyst was then added to the reaction, and the mixture was stirred overnight at 40 °C (55 °C for naphthalene derivatives). Reaction progress was monitored by TLC (*n*-hexane/EtOAc 1:1). After completion, the solvent was evaporated and the obtained residue was suspended in water, extracted with DCM (3x150 mL), the combined organic fractions were washed with brine and dried over anhydrous Na_2SO_4. The crude product obtained after solvent evaporation was purified by flash chromatography (gradient elution, from 100% *n*-hexane to 100% EtOAc over 45 min). The obtained solid product was recrystallized from EtOAc to yield pure final product (yield 23–95%).

4.2. Antimicrobial activity

4.2.1. In vitro antimycobacterial activity

Testing was performed by Microplate Alamar Blue Assay (MABA) according to EUCAST recommendations, where the results were expressed as MIC in μg/mL in comparison with isoniazid (INH), rifampicin (RIF), and ciprofloxacin (CIP) as standards. MIC values were determined in duplicate using two-fold serial dilutions. Replicate determinations were considered acceptable when values were identical or differed by no more than one two-fold dilution step. A full description of the methodology and characterization of the strains is available in Supplementary material S1.

4.2.2. In vitro antibacterial and antifungal activity

The microdilution broth method was performed according to EUCAST recommendations, with slight modifications. Antibacterial and antifungal activities were expressed as MIC. Internal quality standards, gentamicin (GEN), CIP, amphotericin B (AMB), and voriconazole (VRC) were included in the assays. MIC values were determined in duplicate using two-fold serial dilutions. Replicate determinations were considered acceptable when values were identical or differed by no more than one two-fold dilution step. A full description of the methodology and characterization of the used strains is available in Supplementary material S1.

4.3. Toxicity evaluation

4.3.1. Cytotoxicity in HepG2 and HK-2 cells

Cytotoxicity was assessed in HepG2 cells using the CellTiter 96® AQueous One Solution Cell Proliferation Assay (Promega, Madison, WI, USA). Cells were incubated with tested compounds for 24 h, followed by a 2 h incubation with the reagent prior to absorbance measurement at 490 nm. Full experimental details are provided in the Supplementary material S1.

4.3.2. Hemolysis assay (human erythrocytes)

Hemolytic activity was evaluated using human erythrocytes by measuring hemoglobin release at 405 nm. Erythrocytes were incubated with tested compounds at 37 °C for 1 h prior to analysis. Full experimental details are provided in the Supplementary material S1.

4.3.3. In vivo toxicity (Galleria mellonella)

In vivo toxicity was evaluated in the *Galleria mellonella* model following intrahemocoel administration. Larval survival was monitored for up to 5 days post-treatment. Full methodology is described in the Supplementary material S1.

4.4. Mechanism of action (MoA)

4.4.1. The effect on mycolic acids and lipids synthesis

The effect of selected compounds on lipid and mycolic acid biosynthesis in Mtb H37Ra was investigated using our established biochemical assay based on incorporation of ^{14}C-labelled precursor ([^{14}C]-acetate). For details, see Supplementary material S1.

4.4.2. Target overexpression assay

The activity of selected compounds was evaluated against *Mycobacterium tuberculosis* H37Ra strains overproducing key FAS II enzymes, namely enoyl-ACP reductase (InhA) and the β-hydroxyacyl-ACP dehydratase complex (HadABC), using a drop dilution assay. Plates were incubated at 37 °C for 28 days. MIC values were compared to control strains harboring empty vectors. Full details are provided in Supplementary material S1.

4.5. Determination of microsomal stability

Metabolic stability of compounds **7** and **37** was determined in human liver microsomes. Samples were incubated at 25 °C and analyzed at multiple time points (0–45 min) by HPLC-MS. Full experimental details are provided in Supplementary material S1.

Declaration of generative AI and AI-assisted technologies in the manuscript preparation process

During the preparation of this work, the author(s) used ChatGPT (OpenAI) to improve language quality, including grammar, clarity, and typographical corrections. After using this tool, the author(s) reviewed and edited the content as needed and take full responsibility for the content of the published article.

Deposition number

CCDC 2520855 (for compound **37**) contains the supplementary crystallographic data for this paper. These data are provided free of charge by the joint Cambridge Crystallographic Data Centre and Fachinformationszentrum Karlsruhe Access Structures service http://www.ccdc.cam.ac.uk/structures.

Funding

The study was supported by the Grant Agency of Charles University, Project GA UK No. 230 623 (grant to P.A.H.). The study was supported by the project National Institute of Virology and Bacteriology (Programme EXCELES, ID Project No. LX22NPO5103) - Funded by the European Union - Next Generation EU (grant to J. Z.). Additional support was provided by MH CZ-DRO (University Hospital Hradec Králové, Nr. 00179906, grant to M.N.) and by Charles University (SVV 260 666).

CRediT authorship contribution statement

Priam-Amedeo Houngbedji: Conceptualization, Data curation, Formal analysis, Investigation, Methodology, Visualization, Writing – original draft. **Andrea Bachtíková:** Data curation, Investigation, Methodology. **Jarmila Boháčová:** Investigation. **Parinaz Tabarestani:** Investigation. **Ondřej Janďourek:** Investigation, Methodology, Writing – review & editing. **Klára Konečná:** Investigation, Methodology, Validation, Writing – review & editing. **Jan Österreicher:** Investigation, Methodology. **Pavla Paterová:** Investigation, Methodology. **Martin Novák:** Investigation, Methodology, Writing – original draft. **Pavel Bárta:** Investigation, Methodology. **Monika Záhorszká:** Investigation. **Jana Korduláková:** Investigation, Methodology, Writing – original draft. **Matteo Mori:** Data curation, Formal analysis, Investigation, Methodology, Writing – original draft. **Fiorella Meneghetti:** Writing – review & editing. **Jan Zitko:** Conceptualization, Formal analysis, Funding acquisition, Resources, Supervision, Writing – original draft, Writing – review & editing.

Declaration of competing interest

The authors declare that they have no known competing financial interests or personal relationships that could have appeared to influence the work reported in this paper.

Acknowledgements

We thank Ida Dufková and Jana Vacková for help with basic microbiological screening.

Appendix A. Supplementary data

Supplementary data to this article can be found online at https://doi.org/10.1016/j.ejmech.2026.119091.

Data availability

The data supporting this article have been included as part of Supplementary material S1 and Supplementary material S2.

References

[1] Global Tuberculosis Report 2025, World Health Organization, Geneva, 2025. Licence: CC BY-NC-SA 3.0 IGO, https://www.who.int/publications/i/item/9789240116924. (Accessed 6 February 2026).
[2] WHO Operational Handbook on Tuberculosis. Module 4: Treatment and Care, World Health Organization, Geneva, 2025. Licence: CC BY-NC-SA 3.0 IGO, https://www.who.int/publications/i/item/9789240108141. (Accessed 6 February 2026).
[3] K.W. Simranpreet, S. Sangeeta, A.C. Pooja, Anti-tubercular activity of pyrazinamide conjugates: synthesis and structure-activity relationship studies, Mini Rev. Med. Chem. 23 (6) (2023) 700–718, https://doi.org/10.2174/1389557522666220819092431.
[4] E.A. Lamont, N.A. Dillon, A.D. Baughn, The bewildering antitubercular action of pyrazinamide, Microbiol. Mol. Biol. Rev. 84 (2) (2020), https://doi.org/10.1128/mmbr.00070-19.
[5] O. Zimhony, J.S. Cox, J.T. Welch, C. Vilchèze, W.R. Jacobs, Pyrazinamide inhibits the eukaryotic-like fatty acid synthetase I (FASI) of Mycobacterium tuberculosis, Nat. Med. 6 (9) (2000) 1043–1047, https://doi.org/10.1038/79558.
[6] P. Ragunathan, M. Cole, C. Latka, W.W. Aragaw, P. Hegde, J. Shin, M. S. Subramanian Manimekalai, S. Rishikesan, C.C. Aldrich, T. Dick, et al., Mycobacterium tuberculosis PanD structure–function analysis and identification of a potent pyrazinoic acid-derived enzyme inhibitor, ACS Chem. Biol. 16 (6) (2021) 1030–1039, https://doi.org/10.1021/acschembio.1c00131.
[7] M. Dolezal, J. Zitko, Z. Osicka, J. Kunes, M. Vejsova, V. Buchta, J. Dohnal, J. Jampilek, K. Kralova, Synthesis, antimycobacterial, antifungal and photosynthesis-inhibiting activity of chlorinated N-phenylpyrazine-2-carboxamides, Molecules 15 (12) (2010) 8567–8581, https://doi.org/10.3390/molecules15128567.
[8] B. Servusová, J. Vobicková, P. Paterová, V. Kubíček, J. Kuneš, M. Doležal, J. Zitko, Synthesis and antimycobacterial evaluation of N-substituted 5-chloropyrazine-2-carboxamides, Bioorg. Med. Chem. Lett 23 (12) (2013) 3589–3591, https://doi.org/10.1016/j.bmcl.2013.04.021.
[9] J. Zitko, B. Servusová, P. Paterová, J. Mandíková, V. Kubíček, R. Kučera, V. Hrabcová, J. Kuneš, O. Soukup, M. Doležal, Synthesis, antimycobacterial activity and in vitro cytotoxicity of 5-Chloro-N-phenylpyrazine-2-carboxamides, Molecules 18 (12) (2013) 14807–14825, https://doi.org/10.3390/molecules181214807.
[10] B. Servusová, D. Eibinová, M. Doležal, V. Kubíček, P. Paterová, M. Peško, K. Kráľová, Substituted N-Benzylpyrazine-2-carboxamides: synthesis and biological evaluation, Molecules 17 (11) (2012) 13183–13198, https://doi.org/10.3390/molecules171113183.
[11] P.-A. Houngbedji, D.E. Nawrot, O. Janďourek, K. Konečná, M. Novák, P. Paterová, P. Bárta, M.H. Rambaher, E. Novotná, C. Castellano, et al., Investigating the mechanism of antimycobacterial and antiproliferative activity of (E)-N'-Benzylidenepyrazine-2-Carbohydrazides and their derivatives, ChemMedChem 20 (18) (2025) e202500085, https://doi.org/10.1002/cmdc.202500085.
[12] J. Zitko, O. Jand'ourek, P. Paterová, L. Navrátilová, J. Kuneš, J. Vinšová, M. Doležal, Design, synthesis and antimycobacterial activity of hybrid molecules combining pyrazinamide with a 4-phenylthiazol-2-amine scaffold, Medchemcomm 9 (4) (2018) 685–696, https://doi.org/10.1039/C8MD00056E.
[13] K. Bozorov, J. Zhao, H.A. Aisa, 1,2,3-Triazole-containing hybrids as leads in medicinal chemistry: a recent overview, Bioorg. Med. Chem. 27 (16) (2019) 3511–3531, https://doi.org/10.1016/j.bmc.2019.07.005.
[14] K. Barral, A.D. Moorhouse, J.E. Moses, Efficient conversion of aromatic amines into azides: a one-pot synthesis of triazole linkages, Org. Lett. 9 (9) (2007) 1809–1811, https://doi.org/10.1021/ol070527h.
[15] W.J. Chung, A. Kornilov, B.H. Brodsky, M. Higgins, T. Sanchez, L.B. Heifets, M. H. Cynamon, J. Welch, Inhibition of M. tuberculosis in vitro in monocytes and in mice by aminomethylene pyrazinamide analogs, Tuberculosis 88 (5) (2008) 410–419, https://doi.org/10.1016/j.tube.2008.06.001.
[16] M. Marzi, M. Farjam, Z. Kazeminejad, A. Shiroudi, A. Kouhpayeh, E. Zarenezhad, A recent overview of 1,2,3-Triazole-Containing hybrids as novel antifungal agents: focusing on synthesis, mechanism of action, and structure-activity relationship (SAR), J. Chem. 2022 (1) (2022) 7884316, https://doi.org/10.1155/2022/7884316.
[17] C. Deng, H. Yan, J. Wang, K. Liu, B.-s. Liu, Y.-m. Shi, 1,2,3-Triazole-containing hybrids with potential antibacterial activity against ESKAPE pathogens, Eur. J. Med. Chem. 244 (2022) 114888, https://doi.org/10.1016/j.ejmech.2022.114888.
[18] R. Reddyrajula, U. Dalimba, The bioisosteric modification of pyrazinamide derivatives led to potent antitubercular agents: synthesis via click approach and molecular docking of pyrazine-1,2,3-triazoles, Bioorg. Med. Chem. Lett 30 (2) (2020) 126846, https://doi.org/10.1016/j.bmcl.2019.126846.
[19] S.G. Franzblau, R.S. Witzig, J.C. McLaughlin, P. Torres, G. Madico, A. Hernandez, M.T. Degnan, M.B. Cook, V.K. Quenzer, R.M. Ferguson, et al., Rapid, low-technology MIC determination with clinical Mycobacterium tuberculosis isolates by using the microplate Alamar Blue assay, J. Clin. Microbiol. 36 (2) (1998) 362–366, https://doi.org/10.1128/jcm.36.2.362-366.1998.
[20] J. Phelan, A. Maitra, R. McNerney, M. Nair, A. Gupta, F. Coll, A. Pain, S. Bhakta, T. G. Clark, The draft genome of Mycobacterium aurum, a potential model organism for investigating drugs against Mycobacterium tuberculosis and Mycobacterium leprae, Int. J. Mycobacteriol. 4 (3) (2015) 207–216, https://doi.org/10.1016/j.ijmyco.2015.05.001.
[21] I.L. Sparks, K.M. Derbyshire, W.R. Jacobs Jr., Y.S. Morita, Mycobacterium smegmatis: the vanguard of mycobacterial research, J. Bacteriol. 205 (1) (2023) e0033722, https://doi.org/10.1128/jb.00337-22.

[22] M.R. Maleki, S.R. Moaddab, The growing impact of nontuberculous mycobacteria: a multidisciplinary review of ecology, pathogenesis, diagnosis, and treatment, Infectious Medicine 4 (3) (2025) 100203, https://doi.org/10.1016/j.imj.2025.100203.
[23] M.T. Heinrichs, R.J. May, F. Heider, T. Reimers, B.S. Sk, C.A. Peloquin, H. Derendorf, Mycobacterium tuberculosis strains H37ra and H37rv have equivalent minimum inhibitory concentrations to most antituberculosis drugs, Int. J. Mycobacteriol. 7 (2) (2018) 156–161, https://doi.org/10.4103/ijmy.ijmy_33_18.
[24] L. Ryskova, R. Bolehovska, R. Kukla, M. Svarc, A. Zavrelova, H. Vanicek, I. Pavlik, P. Bostik, Mycobacterioses induced by Mycobacterium abscessus: case studies indicating the importance of molecular analysis for the identification of antibiotic resistance, Antibiotics (Basel) 11 (7) (2022) 873, https://doi.org/10.3390/antibiotics11070873.
[25] S. Tunesi, A. Zelazny, Z. Awad, F. Mougari, J.M. Buyck, E. Cambau, Antimicrobial susceptibility of Mycobacterium abscessus and treatment of pulmonary and extra-pulmonary infections, Clin. Microbiol. Infection 30 (6) (2024) 718–725, https://doi.org/10.1016/j.cmi.2023.09.019.
[26] E. Elmorsy, S. Attalla, E. Fikry, A. Kocon, R. Turner, D. Christie, A. Warren, L. Nwidu, W. Carter, Adverse effects of anti-tuberculosis drugs on HepG2 cell bioenergetics, Hum. Exp. Toxicol. 36 (6) (2017) 616–625, https://doi.org/10.1177/0960327116660751.
[27] I.P. Sæbø, M. Bjørås, H. Franzyk, E. Helgesen, J.A. Booth, Optimization of the hemolysis assay for the assessment of cytotoxicity, Int. J. Mol. Sci. 24 (3) (2023) 2914, https://doi.org/10.3390/ijms24032914.
[28] K. Ignasiak, A. Maxwell, Galleria mellonella (greater wax moth) larvae as a model for antibiotic susceptibility testing and acute toxicity trials, BMC Res. Notes 10 (1) (2017) 428, https://doi.org/10.1186/s13104-017-2757-8.
[29] H.I. Boshoff, V. Mizrahi, C.E. Barry, Effects of pyrazinamide on fatty acid synthesis by whole mycobacterial cells and purified fatty acid synthase I, J. Bacteriol. 184 (8) (2002) 2167–2172, https://doi.org/10.1128/jb.184.8.2167-2172.2002.
[30] S.C. Ngo, O. Zimhony, W.J. Chung, H. Sayahi, W.R. Jacobs, J.T. Welch, Inhibition of isolated *Mycobacterium tuberculosis* fatty acid synthase I by pyrazinamide analogs, Antimicrob. Agents Chemother. 51 (7) (2007) 2430–2435, https://doi.org/10.1128/aac.01458-06.
[31] M.H. Larsen, C. Vilchèze, L. Kremer, G.S. Besra, L. Parsons, M. Salfinger, L. Heifets, M.H. Hazbon, D. Alland, J.C. Sacchettini, et al., Overexpression of inhA, but not kasA, confers resistance to isoniazid and ethionamide in Mycobacterium smegmatis, M. bovis BCG and M. tuberculosis, Mol. Microbiol. 46 (2) (2002) 453–466, https://doi.org/10.1046/j.1365-2958.2002.03162.x.
[32] V. Pflégr, L. Horváth, J. Stolaříková, A. Pál, J. Korduláková, S. Bősze, J. Vinšová, M. Krátký, Design and synthesis of 2-(2-isonicotinoylhydrazineylidene) propanamides as InhA inhibitors with high antitubercular activity, Eur. J. Med. Chem. 223 (2021) 113668, https://doi.org/10.1016/j.ejmech.2021.113668.
[33] A.E. Grzegorzewicz, J. Korduláková, V. Jones, S.E. Born, J.M. Belardinelli, A. Vaquié, V.A. Gundi, J. Madacki, N. Slama, F. Laval, et al., A common mechanism of inhibition of the Mycobacterium tuberculosis mycolic acid biosynthetic pathway by isoxyl and thiacetazone, J. Biol. Chem. 287 (46) (2012) 38434–38441, https://doi.org/10.1074/jbc.M112.400994.
[34] E.K. Samani, S.M.N. Hasan, A.F.A. Keszei, M. Heydari, M.T. Mazhab-Jafari, Structural basis of product recognition by Mycobacterium tuberculosis fatty acid synthase, Protein Sci. 35 (1) (2026) e70412, https://doi.org/10.1002/pro.70412.
[35] L. Ciccarelli, Sean R. Connell, M. Enderle, Deryck J. Mills, J. Vonck, M. Grininger, Structure and conformational variability of the Mycobacterium tuberculosis fatty acid synthase multienzyme complex, Structure 21 (7) (2013) 1251–1257, https://doi.org/10.1016/j.str.2013.04.023.
[36] N. Elad, S. Baron, Y. Peleg, S. Albeck, J. Grunwald, G. Raviv, Z. Shakked, O. Zimhony, R. Diskin, Structure of Type-I Mycobacterium tuberculosis fatty acid synthase at 3.3 Å resolution, Nat. Commun. 9 (1) (2018) 3886, https://doi.org/10.1038/s41467-018-06440-6.
[37] H. Sayahi, K.M. Pugliese, O. Zimhony, W.R. Jacobs Jr, A. Shekhtman, J.T. Welch, Analogs of the antituberculous agent pyrazinamide are competitive inhibitors of NADPH binding to M. tuberculosis fatty acid synthase I, Chem. Biodivers. 9 (11) (2012) 2582–2596, https://doi.org/10.1002/cbdv.201200291.